Chemical Science

EDGE ARTICLE

View Article Online
View Journal | View Issue

Cite this: *Chem. Sci.*, 2017, **8**, 6570

The unexpected roles of σ and π orbitals in electron donor and acceptor group effects on the ^{13}C NMR chemical shifts in substituted benzenes†

Renan V. Viesser,[a] Lucas C. Ducati,*[b] Cláudio F. Tormena*[a] and Jochen Autschbach*[c]

Received 14th May 2017
Accepted 20th July 2017

DOI: 10.1039/c7sc02163a

rsc.li/chemical-science

Effects of electron-donating (R = NH_2) and electron-withdrawing (R = NO_2) groups on ^{13}C NMR chemical shifts in R-substituted benzene are investigated by molecular orbital analyses. The ^{13}C shift substituent effect in *ortho*, *meta*, and *para* position is determined by the σ bonding orbitals in the aryl ring. The π orbitals do not explain the substituent effects in the NMR spectrum as conventionally suggested in textbooks. The familiar electron donating and withdrawing effects on the π system by NH_2 and NO_2 substituents induce changes in the σ orbital framework, and the ^{13}C chemical shifts follow the trends induced in the σ orbitals. There is an implicit dependence of the σ orbital NMR shift contributions on the π framework, *via* unoccupied π* orbitals, due to the fact that the nuclear shielding is a response property.

^{13}C NMR chemical shifts can be used to detect substituent effects on aromatic compounds, which, in turn, are associated with the chemical reactivity of the benzene ring in electrophilic aromatic substitutions.[1–3] Benzene ring substituents are classified as activating or deactivating towards electrophilic attack; the former increase the π electron density at the ring whereas the latter decrease it. Moreover, the (de-)activation causes the substituents to be *ortho*-, *meta*-, or *para*-directing.[3] For instance, the NH_2 substituent is activating and *ortho*- and *para*-directing, whereas NO_2 is deactivating and *meta*-directing.[3] The substituent effects are usually divided into inductive (or field-) effects, and resonance (or mesomeric) effects, which are thought to be transmitted *via* the σ and π bonding frameworks, respectively.[4–6] The inductive effect is electron-withdrawing from the aryl ring for both NO_2 and NH_2 but more pronounced for NO_2 because of the combined electronegativity of the nitrogen and oxygen atoms.[7–9]

The contrasting behavior of the two groups toward directing electrophilic substitutions is commonly explained by π-resonance structures, suggesting an accumulation of π electron density at the *ortho* and *para* ring positions in the presence of an NH_2 group, and depletion of π density at the same positions by an NO_2 group.[8,10] Recent computational results by Stasyuk *et al.*[8] utilizing Kohn–Sham (KS) density functional theory and a Voronoi Deformation Density (VDD) charge analysis reinforce these classical arguments and the importance of the π electron delocalization in aniline and nitrobenzene.

The electron-donating and -withdrawing substituent effects in aromatic compounds are associated with pronounced changes in ^{13}C NMR chemical shifts.[11–16] In a simple model, one associates higher electron density with increased magnetic shielding, *i.e.* less positive chemical shifts. Donating electron groups are then expected to shield the carbon nuclei located at *ortho* and *para* positions, whereas withdrawing electron substituents de-shield at the same positions. *meta* positions are usually unaffected by the substituents, in agreement with the model.[1–3] This type of reasoning is often applied to rationalize the effect of substituents on the nuclear shielding at *meta*- and *para*-positions. *ortho*-Positions show a more complex behavior than the *meta* and *para* analogs due to the proximity of the substituent.[17–19] For example, the nitro group causes an increased shielding of *ortho*-carbons instead of the expected de-shielding similar to that taking place at the *para* position.[1,11]

π orbitals are commonly invoked to explain the effects of electron donating and withdrawing groups on the ^{13}C chemical shifts. However, the large shifts of the protons in benzene itself, classically explained by a π ring-current anisotropy model, were shown to be caused by a large magnetic de-shielding from σ orbitals.[20,21] It is not clear from the literature what role the σ orbitals may play in the ^{13}C chemical shift substituent trends, if any, or what the shielding *vs.* de-shielding mechanisms are for each type of orbital symmetry in relation to the substituent

[a]*Institute of Chemistry, University of Campinas – UNICAMP, P. O. Box 6154, 13083-970, Campinas, SP, Brazil. E-mail: tormena@iqm.unicamp.br*

[b]*Department of Fundamental Chemistry, Institute of Chemistry, University of São Paulo, Av. Prof. Lineu Prestes, 748, 05508-000, São Paulo, SP, Brazil. E-mail: ducati@iq.usp.br*

[c]*Department of Chemistry, University at Buffalo, State University of New York, Buffalo, NY 14260-3000, USA. E-mail: jochena@buffalo.edu*

† Electronic supplementary information (ESI) available: Experimental ^{13}C NMR chemical shifts, individual components of the ^{13}C NMR shielding tensor, lists and graphics of NLMO contributions, and tables of NLMO properties. See DOI: 10.1039/c7sc02163a

positions. The present study aims at filling this gap of knowledge, by analyzing results from first-principles calculations for benzene, aniline, and nitrobenzene. Quantum mechanical analyses in terms of 'chemist's orbitals' representing individual bonds, core shells, lone pairs, and antibonding orbitals, gain insight into how stereoelectronic interactions influence the NMR chemical shifts. The results of the analysis appear to be unintuitive, at first, because the σ orbitals are responsible for the known substituent effects in the ^{13}C chemical shifts. However, we also show that there is nonetheless a clear relation between the NMR shift effects and the known chemical effects of the substituents.

Methods

The Amsterdam Density Functional suite (ADF, version 2014)[22–24] was used for all calculations. KS geometry optimizations and ^{13}C NMR shielding tensor calculations were carried out with the PBE0 hybrid functional,[25] the triple-ζ Slater-type atomic orbital (STO) basis with two sets of polarized functions (TZ2P) from the ADF basis set library, recommended options for hybrid functionals, and 'very good' Becke integration grids.[26] The conductor-like screening model (COSMO)[27] with parameters for chloroform was applied to simulate (weak) solvent effects.

^{13}C chemical shifts are referenced to TMS. The ^{13}C shifts δ_i were calculated *via*

$$\delta_i = \sigma_{benz} - \sigma_i + \delta_{benz} \quad (1)$$

where σ_i is the calculated shielding of the carbon nucleus of interest, and σ_{benz} and δ_{benz} are the calculated carbon shielding and the experimental chemical shift with respect to TMS, respectively, of benzene. It is important to note that the trends analyzed herein are not affected by the nature of the intermediate reference.

An NMR shielding analysis was carried out along the lines of ref. 28–30 in terms of natural localized molecular orbitals (NLMOs) generated by the NBO 6.0 program.[31] A synopsis is given below in the context of the present work.

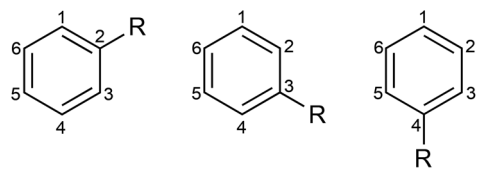

R = H, NH_2, or NO_2

In order to simplify the discussion, the NMR shift is always the one calculated for carbon no. 1 (C1) in the scheme above, with the R-group in *ortho*, *meta*, or *para* position relative to C1. The calculated C1 NMR shielding tensor ($\boldsymbol{\sigma}^{total}$) was decomposed into contributions of the diamagnetic ($\boldsymbol{\sigma}^{dia}$) and paramagnetic ($\boldsymbol{\sigma}^{para}$) mechanisms. The role of the σ and π orbitals was rationalized *via* analyses of $\boldsymbol{\sigma}^{total}$, and its dia and para contributions, in terms of individual orbitals. The effect of the magnetic field orientation relative to the molecule was analyzed by considering the principal components σ_{11}, σ_{22} and σ_{33} of the shielding tensor in its molecule-fixed principal axis system (PAS). For R-benzene, the σ_{11} and σ_{22} components of the C1 shielding tensor lie in the aryl ring plane, while the most positive tensor component, σ_{33}, is perpendicular to the aryl ring plane. The contributions and the complete set of shielding analysis data is provided in the ESI, Tables S3 and S4.†

Atomic charges were calculated by the Voronoi Deformation Density (VDD)[8,32,33] partitioning. Molecular structures were optimized with C_s symmetry to allow a decomposition of the total charges into a' and a'' irreducible representations, corresponding to the σ and π frameworks, respectively. To analyze the charge rearrangements on the benzene ring caused by the R substituents, Ph$^\bullet$ and R$^\bullet$ radical fragments were generated using a restricted open-shell KS approach.

Results and discussion

The calculated and experimental ^{13}C NMR chemical shifts (Table S1†) show good agreement with the experimental data (Fig. 1). The calculated and experimental shifts deviate from each other by no more than 2%, which is acceptable. Importantly, the experimentally observed trends are faithfully reproduced by the calculations, which means that a meaningful analysis of the trends can be carried out at the chosen level of theory.

Relative to benzene, the carbon nuclei have smaller shifts upon NH_2 substitution in *ortho* and *para* positions. The NH_2 group effect is larger for *ortho* than *para*. Relative to benzene, the NO_2 substituent causes opposite effects for the *ortho* and *para* positions: the carbon shift becomes larger with NO_2 in the *para* position, while the shift decreases in the *ortho* position. The carbon shifts in *meta* position are hardly affected by the substituents.

In the following, we focus on the nuclear magnetic shielding rather than the chemical shift, as it is the more fundamental physical quantity. The shift and shielding scales have opposite signs (eqn (1)). To re-state the trends in terms of shielding:

(1) Relative to benzene, the NH_2 substituent causes increased shielding both in *ortho* and *para* positions.

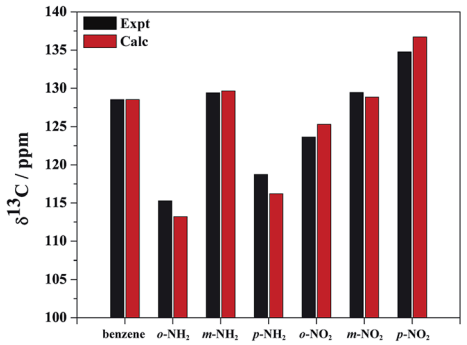

Fig. 1 Calculated (Calc) and experimental (Expt) carbon 1 (C1) isotropic ^{13}C NMR chemical shifts for benzene, NH_2–benzene, and NO_2–benzene. *ortho* (*o*-), *meta* (*m*-), and *para* (*p*-) correspond to the C1 position relative to R.

(2) Relative to benzene, the NO_2 substituent causes increased shielding of in *ortho* and de-shielding in *para* position.

It is important to keep in mind that the terms paramagnetic and diamagnetic are used to refer to different (although somewhat arbitrarily defined) mechanisms that contribute to the total shielding, not the sign of observed trends in the shielding constants or chemical shifts among the set of compounds. However, the diamagnetic shielding is indeed positive for carbon and tends to vary comparatively little among different compounds, while the paramagnetic contribution is usually negative and determines the magnitude and direction of the chemical shift.

The observed shielding trends are indeed associated with the paramagnetic shielding mechanism (Table S2†). In KS theory, the paramagnetic shielding can be expressed in terms of canonical molecular orbitals (CMOs, the 'usual' orbitals from self-consistent field KS calculations) for each tensor element $\sigma_{u,v}$, with $u,v \in \{x, y, z\}$, as[30]

$$\sigma_{u,v}^{\text{para}} = \text{const.}\ \text{Re}\sum_{i}^{\text{occ}}\sum_{a}^{\text{unocc}}\frac{\left\langle\varphi_i\middle|\hat{F}_u^{\text{OZ}}\middle|\varphi_a\right\rangle\left\langle\varphi_a\middle|\hat{h}_v^{\text{PSO}}\middle|\varphi_i\right\rangle}{\varepsilon_i-\varepsilon_a} \qquad (2)$$

here, φ_i, ε_i and φ_a, ε_a represent occupied and unoccupied KS CMOs and their energies, respectively. The superscript OZ refers to the orbital Zeeman perturbation due to the external magnetic field. The superscript PSO refers to the paramagnetic nuclear spin – electron orbital perturbation due to the nuclear spin hyperfine magnetic field. Further, $\hat{F}$ and $\hat{h}$ are the KS Fock operator and its one-electron part. The OZ and PSO perturbations of $\hat{F}$ and $\hat{h}$ may be swapped. Irrespective of whether the shielding analysis is carried out in terms of canonical or localized orbitals, eqn (2) indicates that the paramagnetic shielding is associated with magnetic coupling between occupied and unoccupied orbitals, represented by the OZ and PSO matrix elements in the numerators, and the energy gaps between occupied and unoccupied orbitals in the denominators. In the NLMO analysis, the summation over unoccupied orbitals is absorbed into the contributions from each occupied NLMO after transforming the occupied CMO set to the NLMOs.

Both the OZ and PSO matrix elements involve orbital angular momentum operators, because the associated magnetic moments are proportional to the angular momentum (for closed-shell molecules with light elements, the electron spin magnetic moments do not contribute to the shielding). However, in the PSO operators the angular momentum is weighted by the inverse-cube of the electron-nucleus distance. Therefore, the PSO operators mainly sample the electronic structure around the nucleus of interest. The action of a component of the angular momentum operator on an atomic orbital (AO) can be represented by a rotation of the AO (*e.g.* 90° for a 2p AO) or it gives zero (*e.g.* $\hat{L}_z p_z$). In order for a matrix element $\langle\text{unocc}|\hat{h}_v^{\text{PSO}}|\text{occ}\rangle$ to be large, one therefore has to consider the action of an angular momentum component v on the part of the occupied orbital that is centered around the NMR nucleus, and whether the resulting 'rotated' orbital has a large overlap with an unoccupied orbital around the same nucleus. The associated paramagnetic shielding contribution, usually negative, is particularly large if the two orbitals are close in energy. This type of analysis for the paramagnetic shielding is sometimes referred to as an 'orbital rotation model'.[34] Note that such models usually rely on a σ/π partitioning of the molecular orbitals, and consequently we used LMOs that have the same partitioning. We do not expect our results to change qualitatively if a different localization technique is used, as long as the localization also gives σ and π orbitals and not the 'banana bond' orbitals for multiple bonds that are produced by some orbital localization methods. (Using one of the latter would also not allow us to make connections with the textbook explanations for the shielding trends, and therefore not be suitable for the present study.)

Only very few orbitals dictate the R effects in the isotropic shielding in R–benzene, as shown in Fig. 2 by comparing the full substituent effects (*i.e.* from all NLMOs) with the added contributions from just the three σ-bonding NLMOs σ_{C1-C2}, σ_{C1-C6}, and σ_{C1-H}. This simplifies the analysis considerably. Fig. 2 also implies that the σ framework of orbitals is predominantly responsible for the substituent effects on the NMR carbon shifts, not the π system. We consider this one of the main findings of the present study.

Further analysis reveals that the substituent effects are associated predominantly with the in-plane principal shielding components (σ_{11} and σ_{22}). The σ_{11}, σ_{22}, and σ_{33} components are listed in Table 1. The σ_{11} trends are associated with the σ_{C1-C} NLMOs, while the variations in σ_{22} are associated with the σ_{C1-H} NLMO. (Sometimes, a shielding analysis in terms of CMOs can also be very insightful,[35] in particular when shielding effects can be tied to the orbital energy gaps $\Delta\varepsilon_{i,a} = \varepsilon_i - \varepsilon_a$ in the denominator of eqn (2). We also performed the shielding analysis in terms of CMOs, but decided to forgo a discussion because the trends were less clear, mainly due to the fact that multiple occupied and unoccupied CMOs contribute to the shielding trends and no obvious relationship to the $\Delta\varepsilon_{i,a}$ could be identified.) The reason why these different orbitals contribute to the trends in $\boldsymbol{\sigma}^{\text{para}}$ *via* different principal components, *i.e.* due to different orientations of the magnetic fields in the aryl plane, is

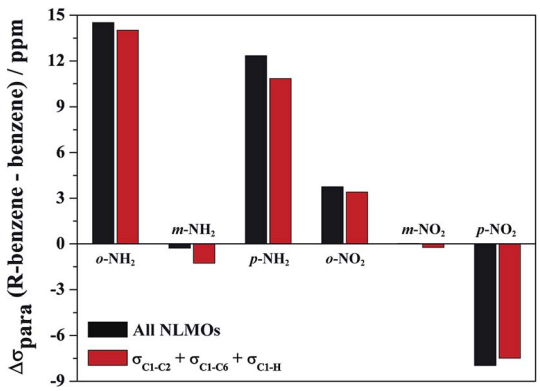

Fig. 2 Sum of all orbital contributions (all occupied NLMOs) and of only the σ_{C1-C2}, σ_{C1-C6}, and σ_{C1-H} contributions to the isotropic part of $\boldsymbol{\sigma}^{\text{para}}$ term of the C1 shielding for R–benzenes (ppm). *ortho* (*o*-), *meta* (*m*-), and *para* (*p*-) is the C1 position relative to R. Shielding relative to benzene at 0 ppm.

Table 1 Sum of σ_{C1-C2}, σ_{C1-C6}, and σ_{C1-H} NLMO contributions to the σ_{11}, σ_{22}, and σ_{33} principal components of the C1 paramagnetic shielding of R–benzenes (ppm). *ortho* (*o*-), *meta* (*m*-), and *para* (*p*-) is the C1 position relative to R

		R						
Component	Orbitals[a]	H	*o*-NH_2	*m*-NH_2	*p*-NH_2	*o*-NO_2	*m*-NO_2	*p*-NO_2
σ_{11}	$\sigma_{C1-C2/6}$	−263.14	−232.79	−266.12	−245.88	−250.64	−261.42	−273.03
σ_{22}	σ_{C1-H}	−208.88	−188.11	−210.25	−195.31	−216.16	−212.21	−222.95
σ_{33}		−40.69	−49.75	−40.13	−38.97	−35.66	−39.79	−39.16

[a] Orbitals responsible for the variations in the shielding tensor components depending on the substituent and position relative to C1.

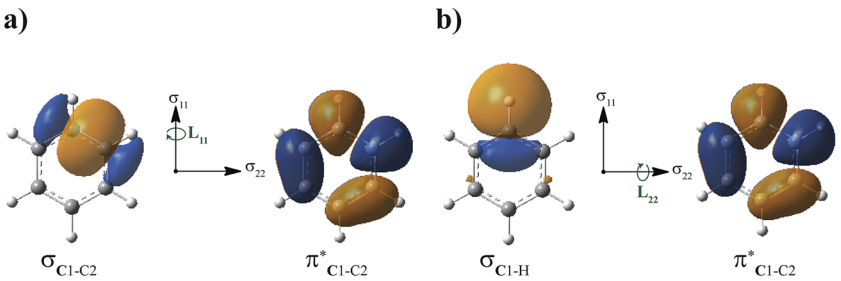

Fig. 3 Isosurfaces (±0.03 au) of σ_{C1-C2} (a) and σ_{C1-H} (b) NLMOs that may rotate around C1 under the action of the angular momentum/magnetic moment operator (*L*) and overlap with the π^*_{C1-C2} unoccupied orbital. This overlap indicates paramagnetic coupling of σ and π* orbitals.

illustrated by Fig. 3. σ_{C1-C} and σ_{C1-H} rotations around the respective principal axis, associated with the action of the magnetic field, produce rotated NLMOs that overlap effectively with the same low-energy π^*_{C1-C2} unoccupied orbital. These overlaps go along with strong magnetic couplings resulting in important contributions to $\boldsymbol{\sigma}^{para}$ from the different magnetic field directions and orbitals.

To analyze the effect of the R substituents on the σ and π system of the benzene ring, we follow the strategy of Stasyuk *et al.*[8] and investigate the electron density rearrangement caused by the R-substitution with the VDD charge analysis method. Fig. 4 displays the σ and π contributions of VDD atomic charges for NH_2– and NO_2–benzene calculated relative to phenyl and substituent fragments. The VDD charge of an atom is the electron deformation density $\Delta\rho = \rho$(R–benzene) − ρ(fragments), times $-e$, integrated over the atomic volume defined by a Voronoi partitioning of the molecule.

NH_2 and NO_2 substituents are known to be electron-donating and electron-withdrawing, respectively, with respect to the aryl π system, which is reflected in the charge analysis. Fig. 4 shows that the NH_2 substituent increases the π density on carbon atoms in the *ortho* and *para* positions, whereas the NO_2 group causes a depletion of π density at the same positions. We obtain similar values as Stasyuk *et al.*[8] using the VDD technique and therefore our conclusions are in line with the reference.

Regarding the σ system, the charge analysis shows the opposite behavior to the π system (also observed by Stasyuk *et al.*).[8] While the NH_2 group causes a depletion of density at carbon atoms in *ortho* and *para* position, an accumulation takes place at the same positions for NO_2 substitution. Carbon atoms in the *meta* positions are basically unaffected by the substitutions. The charge rearrangements in the σ system are only partially explained by the inductive effects of R. The fact that the σ charges are large for the *ortho* and *para* positions but negligible for *meta*, instead of simply decreasing in magnitude with the distance from the substituent, means that there is an energetic stabilization going along with a partial neutralization of the charge rearrangements in the π system by the σ system.

The depletion of σ electron density caused by the NH_2 group in *ortho* and *para* positions leads to a magnitude reduction of the magnetic coupling between $\sigma_{C1-C,H}$ and π^*_{C1-C2} in the paramagnetic shielding. This is clear from Fig. 3. The weight of these occupied orbitals around C1 decreases upon substitution (in Fig. 4, C1 is one of the carbons not bound to the substituent). The reduced weight decreases the overlap of the magnetic-field 'rotated' σ orbitals with the π* orbital, and therefore it reduces the magnetic coupling in the paramagnetic shielding. Accordingly, in Table 1, both the σ_{C1-C} and σ_{C1-H} NLMO contributions to the $\boldsymbol{\sigma}^{para}$ term are less negative when the NH_2 group is in *ortho* and *para* position rather than *meta*. Therefore, the known effect of the NH_2 group, *i.e.* increased *ortho* and *para* shielding, is actually a reduction of de-shielding contributions from the σ system. The larger reduction of electron density in *ortho* position correlates with the stronger substituent shielding effect in *ortho* position. For the *meta* position, the negligible charge effects agree with the similar carbon shielding in benzene *vs.* the substituted systems.

Despite this increased *ortho* and *para* shielding being tied to the occupied σ orbitals, we can connect the less effective paramagnetic mechanism of the σ_{C1-C} and σ_{C1-H} orbitals with the π orbitals as well, in an indirect fashion. Since the π electron density is increased in the *ortho* and *para* positions, *via* shifting weights toward C1 in the occupied π orbitals, the low-energy unoccupied π orbitals must undergo shifts in the reverse.

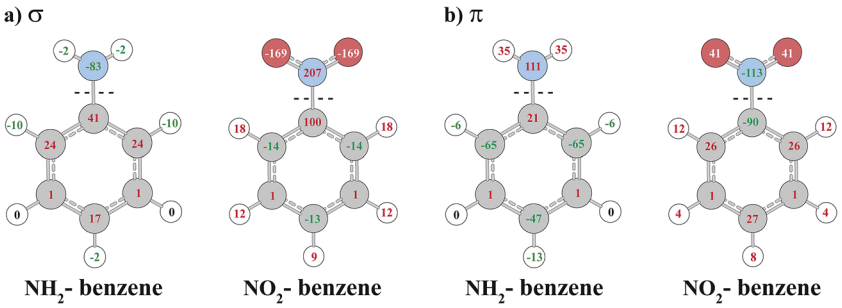

Fig. 4 VDD atomic deformation charges (in 10^{-3}e) for NH_2– and NO_2–benzene calculated relative to fragments. Negative values mean an accumulation of electron density (negative charge), positive values denote electron density depletion (positive charge). Atomic deformation charges are partitioned into σ (panel a) and π (panel b) contributions upon the C–N bond formation.

Referring again to Fig. 3, the combined σ and π effect in the occupied orbital set decreases the C1 weight in the occupied magnetic-field perturbed σ orbitals and in the unoccupied π orbital in the magnetic coupling matrix elements entering $\boldsymbol{\sigma}^{para}$. Therefore, the π accumulation of electron density in the *ortho* and *para* positions has an effect on the magnetic response of the occupied σ orbitals *via* magnetic coupling with low-energy π orbitals, reinforcing the reduced weight effects from the σ orbitals.

Electron density patterns at the carbon atoms upon substitution also describe the effect of NO_2 group in *para* position. As the NO_2 substituent increases the σ electron density at the *para* carbon atom, the magnetic couplings between $\sigma_{C1-C,H}$ and π^*_{C1-C2} are intensified (Fig. 3) and large negative contributions are found for the $\boldsymbol{\sigma}^{para}$ term. This behavior is seen for both σ_{C1-C} and σ_{C1-H} NLMOs (Table 1). Accordingly, the NO_2 group in *para* position causes a de-shielding of C1, while in *meta* there is little effect. As in the case of the NH_2 substituent (but with an opposite trend), the density changes from the occupied π orbitals cause reverse effects in the low-energy π* orbitals, which reinforce the paramagnetic perturbations of the σ framework.

The increased C1 shielding effect of the NO_2 substituent in *ortho* position requires further explanation. According to the overall VDD σ charge (and, indirectly, the π charge), an increase of the paramagnetic de-shielding would be expected. However, the calculated shielding displays the opposite behavior. Table 2 collects individual shielding contributions of the $\sigma_{C1-C,H}$ NLMOs. It is seen that σ_{C1-C2} is responsible for the positive shielding effect of the NO_2 substituent in *ortho* position, relative to benzene. In contrast, σ_{C1-C6} and σ_{C1-H} display similar de-shielding trends as found for the *para* position. In fact, the weight of C1 in these orbitals (ESI, Tables S5–S7†) shows that the overall σ density accumulation in *ortho* position is caused by σ_{C1-C6} and σ_{C1-H}, whereas σ_{C1-C2} is associated with a depletion of electron density. The calculated trends in Table 2 are therefore fully compatible with the C1 weight argument (Fig. 3) used to rationalize the *o*,*m*,*p*-NH_2 and *p*-NO_2 effects.

The peculiar influence of σ_{C1-C2} is explained as follows: C1 is the NMR nucleus, and for *ortho* substitution C2 is the carbon bound to the nitro group. Fig. 4 shows that the inductive σ effect of NO_2 is particularly large at C2 (0.1 electron density depletion), due to the strong electron-withdrawing inductive effect of the NO_2 group. This goes along with a considerable polarization of σ_{C1-C2}, shifting the weight from C1 to C2, as shown in Table S5 in the ESI.† While there is an overall increase of the σ electron density on C1, the σ_{C1-C2} polarizes in the opposite way. The reduced $\boldsymbol{\sigma}^{para}$ de-shielding caused by the σ_{C1-C2} bond outweighs the contributions from all other orbitals. Accordingly, the NO_2 group causes an increased shielding in *ortho* position.

Table 2 σ_{C1-C2} and σ_{C1-C6} NLMO contributions to the σ_{11} shielding component, and σ_{C1-H} NLMO contributions to the σ_{22} component of the $\boldsymbol{\sigma}^{para}$ term of the C1 shielding tensor for benzene and NO_2–benzene (ppm). *ortho* (*o*-), *meta* (*m*-), and *para* (*p*-) is the C1 position relative to R

	R			
NLMO	H	*o*-NO_2	*m*-NO_2	*p*-NO_2
σ_{C1-C2}	−131.60	−116.49	−129.70	−136.54
σ_{C1-C6}	−131.60	−133.87	−131.77	−136.54
σ_{C1-H}	−140.42	−144.75	−142.82	−152.35

Conclusions

The σ bonding orbitals spanning the C1 carbon of interest (σ_{C1-C2}, σ_{C1-C6}, and σ_{C1-H}) are identified as responsible for the NMR shielding/de-shielding effects caused by π electron donating and withdrawing substituents depending on their position relative to C1. The π orbitals do not explain these effects, as conventionally suggested in chemistry textbooks, for two reasons: (i) the nuclear magnetic shielding is not related to the electron density in a simple way because it is a response property. Charge accumulation/depletion arguments must be made on a per-orbital basis and potentially take into account the corresponding effects on low lying unoccupied orbitals. (ii) Electron deformation density patterns induced in the π system by electron donating or withdrawing groups cause a mirror pattern in the σ system that is crucial to understand the related NMR shielding effects.

Because of the magnetic coupling of occupied σ with unoccupied π orbitals in the paramagnetic shielding mechanism, there are additional implicit dependencies of the C1 shielding

on the deformation density patterns induced by the R-substituents. For example, the substituent effects on the occupied π orbitals affect the low-energy unoccupied π* orbitals, which couple magnetically with the occupied σ orbitals. The π* trends reinforce those in the occupied σ orbitals. For NO_2, the increased shielding in *ortho* position is caused by a polarization of the C1–C2 σ bond toward the substituent, despite the electron deformation density indicating an overall σ accumulation at C1.

In summary, the classical organic chemistry concepts about the reactivity and regioselectivity of the benzene ring in electrophilic aromatic substitutions are not in a simple way related to the carbon NMR chemical shifts. However, the analysis shows that in a more indirect way there is an obvious relationship. A study of both the σ and π orbital sets is needed in order to relate the carbon chemical shift trends to the π electron density accumulation and depletion patterns in the substituted benzene rings. Since the *ortho–meta–para* patterns in the π electron density cause mirroring changes in the σ framework, the chemical effects of the R groups that manifest in electrophilic substitutions are ultimately responsible for the observed ^{13}C NMR shifts. These effects persist in multi-substituted benzenes, *e.g.* with additional halogen groups, as we will report in a follow-up study.

Acknowledgements

We acknowledge FAPESP for financial support (2011/17357-3, 2013/03477-2, and 2015/08541-6), scholarships to R. V. V. (2012/12414-1 and 2015/20106-3) and a fellowship to L. C. D. (2014/21930-9). We are grateful for fellowships from CNPq to C. F. T. and L. C. D. (202068/2015-3). J. A. acknowledges the National Science Foundation (CHE-1560881) for financial support. The authors thank the Center for Computational Research (CCR) at the University at Buffalo for providing computational resources. Thanks are extended to Dr Célia Fonseca Guerra for providing information about the VDD analysis.

References

1 N. E. Jacobsen, *NMR Spectroscopy Explained: Simplified Theory, Applications and Examples for Organic Chemistry and Structural Biology*, John Wiley & Sons, Hoboken, USA, 2007.
2 J. H. Simpson, *Organic Structure Determination Using 2-D NMR Spectroscopy*, Elsevier, Oxford, UK, 2008.
3 J. Clayden, N. Greevs, S. Warren and P. Wothers, *Organic Chemistry*, Oxford University Press, USA, 1st edn, 2000.
4 F. A. Carey and R. J. Sundberg, *Advanced Organic Chemistry, Part A: Structure and Mechanisms*, Springer, New York, USA, 5th edn, 2007.
5 T. M. Krygowski and W. P. Oziminski, Substituent effects in 1-nitro-4-substituted bicyclo[2.2.2]octane derivatives: inductive or field effects?, *J. Mol. Model.*, 2014, **20**, 2352.
6 M. Palusiak, M. Domagała, J. Dominikowska and F. M. Bickelhaupt, The substituent effect on benzene dications, *Phys. Chem. Chem. Phys.*, 2014, **16**, 4752–4763.
7 A. R. Campanelli, A. Domenicano, F. Ramondo and I. Hargittai, Group electronegativities from benzene ring deformations: A quantum chemical study, *J. Phys. Chem. A*, 2004, **108**, 4940–4948.
8 O. A. Stasyuk, H. Szatylowicz, T. M. Krygowski and C. Fonseca Guerra, How amino and nitro substituents direct electrophilic aromatic substitution in benzene: An explanation with Kohn-Sham molecular orbital theory and Voronoi deformation density analysis, *Phys. Chem. Chem. Phys.*, 2016, **18**, 11624–11633.
9 H. Szatylowicz, O. A. Stasyuk, C. Fonseca Guerra and T. M. Krygowski, Effect of intra- and intermolecular interactions on the properties of para-substituted nitrobenzene derivatives, *Crystals*, 2016, **6**, 29.
10 H. Zhang, X. Jiang, W. Wu and Y. Mo, Electron conjugation versus π-π repulsion in substituted benzenes: why the carbon-nitrogen bond in nitrobenzene is longer than in aniline, *Phys. Chem. Chem. Phys.*, 2016, **18**, 11821–11828.
11 D. Rasala and R. Gawinecki, 13C NMR study of the substituent effects in ortho-substituted nitrobenzenes, *Magn. Reson. Chem.*, 1992, **30**, 740–745.
12 D. Rasala and R. Gawinecki, Effect of the ortho-nitro group on the 13C NMR chemical shifts of substituted pyridines, *Magn. Reson. Chem.*, 1993, **31**, 38–44.
13 A. Zakrzewska, R. Gawinecki, E. Kolehmainen and B. Ośmiałowski, 13C-NMR based evaluation of the electronic and steric interactions in aromatic amines, *Int. J. Mol. Sci.*, 2005, **6**, 52–62.
14 E. Dumont and P. Chaquin, Investigation of pure inductive effects on benzene ring by 13C NMR chemical shifts: A theoretical study using fictitious nuclear charges of hydrogen atoms ('H* method'), *Chem. Phys. Lett.*, 2007, **435**, 354–357.
15 R. P. Verma and C. Hansch, Use of 13C NMR chemical shift as QSAR/QSPR descriptor, *Chem. Rev.*, 2011, **111**, 2865–2899.
16 G. Chen, X. Wu, C. Cao, F. Liu, R. Zeng and W. Liu, A QSPR correlation on the 13C NMR chemical shifts of bridge carbons for different series of aromatic Schiff bases, *Magn. Reson. Chem.*, 2015, **53**, 172–177.
17 S. Arunima and N. D. Kurur, Ortho effect in fluorobenzenes: Cross-correlated relaxation and quantum chemical studies, *Magn. Reson. Chem.*, 2005, **43**, 132–138.
18 V. Nummert, M. Piirsalu, V. Mäemets, S. Vahur and I. A. Koppel, Effect of ortho substituents on carbonyl carbon 13C NMR chemical shifts in substituted phenyl benzoates, *J. Phys. Org. Chem.*, 2009, **22**, 1155–1165.
19 S. K. Sen Gupta and R. Shrivastava, Solvent sensitivity of ortho substituent effect on 13C NMR chemical shift of the carboxyl carbon (δ CO) in benzoic acid, *Magn. Reson. Chem.*, 2011, **49**, 700–704.
20 M. Baranac-Stojanović, New insight into the anisotropic effects in solution-state NMR spectroscopy, *RSC Adv.*, 2014, **4**, 308–321.
21 M. Baranac-Stojanović, A. Koch and E. Kleinpeter, Is the conventional interpretation of the anisotropic effects of C=C double bonds and aromatic rings in NMR spectra in

terms of the π-electron shielding/deshielding contributions correct?, *Chem.–Eur. J.*, 2012, **18**, 370–376.

22 E. J. Baerends, T. Ziegler, J. Autschbach, D. Bashford, A. Bérces, F. M. Bickelhaupt, C. Bo, P. M. Boerrigter, L. Cavallo, D. P. Chong, L. Deng, R. M. Dickson, D. E. Ellis, M. van Faassen, L. Fan, T. H. Fischer, C. Fonseca Guerra, A. Ghysels, A. Giammona, S. J. A. van Gisbergen, A. W. Götz, J. A. Groeneveld, O. V. Gritsenko, M. Grüning, S. Gusarov, F. E. Harris, P. van den Hoek, C. R. Jacob, H. Jacobsen, L. Jensen, J. W. Kaminski, G. van Kessel, F. Kootstra, A. Kovalenko, M. V. Krykunov, E. van Lenthe, D. A. McCormack, A. Michalak, M. Mitoraj, J. Neugebauer, V. P. Nicu, L. Noodleman, V. P. Osinga, S. Patchkovskii, P. H. T. Philipsen, D. Post, C. C. Pye, W. Ravenek, J. I. Rodríguez, P. Ros, P. R. T. Schipper, G. Schreckenbach, J. S. Seldenthuis, M. Seth, J. G. Snijders, M. Solà, M. Swart, D. Swerhone, G. te Velde, P. Vernooijs, L. Versluis, L. Visscher, O. Visser, F. Wang, T. A. Wesolowski, E. M. van Wezenbeek, G. Wiesenekker, S. K. Wolff, T. K. Woo and A. L. Yakovlev, Amsterdam Density Functional, SCM, *Theoretical Chemistry*, Vrije Universiteit, Amsterdam, The Netherlands, http://www.scm.com, accessed 03/17.

23 G. te Velde, F. M. Bickelhaupt, E. J. Baerends, S. J. A. van Gisbergen, C. Fonseca Guerra, J. G. Snijders and T. Ziegler, Chemistry with ADF, *J. Comput. Chem.*, 2001, **22**, 931–967.

24 C. Fonseca Guerra, J. G. Snijders, G. Te Velde and E. J. Baerends, Towards an order-N DFT method, *Theor. Chem. Acc.*, 1998, **99**, 391.

25 C. Adamo and V. Barone, Toward reliable density functional methods without adjustable parameters: The PBE0 model, *J. Chem. Phys.*, 1999, **110**, 6158–6170.

26 M. Franchini, P. H. T. Philipsen and L. Visscher, The Becke fuzzy cells integration scheme in the Amsterdam Density Functional program suite, *J. Comput. Chem.*, 2013, **34**, 1819–1827.

27 A. Klamt and G. Schüürmann, COSMO: A new approach to dielectric screening in solvents with explicit expressions for the screening energy and its gradient, *J. Chem. Soc., Perkin Trans. 2*, 1993, 799–805.

28 J. A. Bohmann, F. Weinhold and T. C. Farrar, Natural chemical shielding analysis of nuclear magnetic resonance shielding tensors from gauge-including atomic orbital calculations, *J. Chem. Phys.*, 1997, **107**, 1173–1184.

29 J. Autschbach, Analyzing NMR shielding tensors calculated with two–component relativistic methods using spin–free localized molecular orbitals, *J. Chem. Phys.*, 2008, **128**, 164112.

30 J. Autschbach and S. Zheng, Analyzing Pt chemical shifts calculated from relativistic density functional theory using localized orbitals: The role of Pt lone pairs, *Magn. Reson. Chem.*, 2008, **46**, S48–S55.

31 E. D. Glendening, J. K. Badenhoop, A. E. Reed, J. Ė. Carpenter, J. A. Bohmann, C. M. Morales and F. Weinhold, *NBO 6.0, theoretical chemistry institute*, University of Wisconsin, Madison, 2013. http://nbo.chem.wisc.edu, accessed 03/17.

32 C. Fonseca Guerra, J.-W. Handgraaf, E. J. Baerends and F. M. Bickelhaupt, Voronoi Deformation Density (VDD) charges: assessment of the Mulliken, Bader, Hirshfeld, Weinhold, and VDD methods for charge analysis, *J. Comput. Chem.*, 2004, **25**, 189–210.

33 L. Guillaumes, S. Simon and C. Fonseca Guerra, The role of aromaticity, hybridization, electrostatics, and covalency in resonance-assisted hydrogen bonds of adenine-thymine (AT) base pairs and their mimics, *ChemistryOpen*, 2015, **4**, 318–327.

34 J. B. Grutzner, Chemical shift theory. Orbital symmetry and charge effects on chemical shifts, in *Recent advances in organic NMR spectroscopy*, Norell Press, Landisville, NJ, 1987, pp. 17–42.

35 S. Berger, U. Fleischer, C. Geletneky and J. C. W. Lohrenz, The 13C chemical shift of the ipso carbon atom in phenyllithium, *Chem. Ber.*, 1995, **128**, 1183–1186.

